Plasmon-phonon-coupled modes and their lineshapes for a doped semiconductor superlattice

Plasmon–phonon-coupled modes and their lineshapes for a doped semiconductor superlattice

A C Sharma† and R Sen‡

† Physics Department, Faculty of Science, M. S. University of Baroda, Vadodara-390002, India
‡ School of Studies in Physics, Jiwaji University, Gwalior-474011, India

Abstract. We studied the plasma oscillations of an electron gas and a hole gas in a GaAs doped superlattice. The doped superlattice is modelled to be a one-dimensional periodic sequence of electron and hole layers which are embedded alternately in a homogeneous polar dielectric host medium. The density–density correlation function has been calculated for a model structure in order to study the plasma–phonon-coupled modes. The strong charge carrier–impurity scattering which results from random doping impurities in the electron (hole) layers, has been taken into account by choosing appropriate polarizabilities for intrasubband–intersubband transitions and the harmonic oscillator wavefunctions as electron (hole) envelope functions. Our calculation demonstrates that the presence of random doping impurities in electron (hole) layers significantly affects both electron and hole plasmons. The well behaved plasma modes in a GaAs doped superlattice can be observed for restricted values of wavevector. In the 2D limiting case, the plasma frequency in a doped superlattice is approximately proportional to $(q^2 - q_c^2)^{1/2}$, while for a modulation doped superlattice (such as $Ga_x In_{1-x} As/GaAs_y Sb_{1-y}$) it is proportional to q, for small q-values. q_c is the critical value of the in-plane wavevector q. Our calculated lineshapes of coupled plasmon–phonon modes can be well separated from each other and could have reasonable half-widths and peak heights which could be observed experimentally for the right choice of values for the parameters of the doped superlattice.

1. Introduction

A doped semiconductor superlattice (DSSL) consists of a one-dimensional periodic sequence of alternating doping of impurities in a homogeneous dielectric background. The periodic potential in a DSSL is caused by the space-charge-induced potential of the doped ionized impurity, and it originates from the band-gap discontinuity in the case of a compositional semiconductor superlattice (CSSL). The space-charge potential in a DSSL modulates the band edges of the host material such that nearly perfect separation of electrons and holes can be achieved. The electron–hole recombination lifetimes can therefore be greatly enhanced by the right choice of design parameters, such as the doping concentrations and the electron (hole) layer thickness [1, 2]. The separation of the electron (hole) into narrow layers causes splitting of conduction and valence bands into quasi-two-dimensional (2D) subbands, whose spacing can be tailored by choosing appropriate design parameters. Therefore, a quantum phenomenon can be observed very well in a DSSL [3, 4].

The plasma frequency is one of the key parameters in characterizing a material. A study of plasmons and the plasmon–phonon-coupled modes reveals several inherent characteristics of a material. In view of this, numerous experimental as well as theoretical studies of plasmons and plasmon–phonon-coupled modes have been performed for modulation doped

CSSLs [5–16]. However, relatively less attention has been paid to both experimental and theoretical studies of plasmons and plasmon–phonon-coupled modes in a DSSL. This might be because of suspected unfavourable properties associated with the diffusion of doped impurities which act as centres of free-carrier scattering [17]. Detailed theoretical studies on the electronic and optical properties of a DSSL show that, in spite of impurity scattering, well behaved plasmon modes could be observed in a DSSL because of the tunable carrier density and the nearly perfect separation of electrons and holes [3, 4, 17]. It has been demonstrated that, for a 2D electron gas consisting of a random impurity potential, plasma oscillations can be observed for reasonably high values of carrier density for restricted values of the wavevector [18]. At small carrier densities, the system enters into a diffusive regime of carrier dynamics which prohibit collective excitations of carriers. Another notable difference between a DSSL and a CSSL is the electron (hole) layer boundaries. Unlike a CSSL, the electron (hole) layer boundaries in a DSSL are not abrupt.

We present in this paper a model calculation of the density–density correlation function (DDCF), for a GaAs DSSL, to study the plasmon–phonon-coupled modes and their lineshapes. We make the following assumptions.

(i) the DSSL can be modelled to be infinite periodic sequence of electron and hole layers embedded alternately in a polarizable host media of dielectric function $\varepsilon(\omega)$ and of a unit cell (which comprises one electron and one hole layer) of length d along the z axis.

(ii) The electrons and holes in the GaAs DSSL are mainly confined to their respective layers and their motion along the z axis can be described with the use of wavefunctions and energy eigenvalues of the harmonic oscillator.

(iii) Confinement of electrons (holes) results in the well separated 2D energy subbands which can be represented by 2D free-electron-like bands of effective mass m_e^* for an electron and m_h^* for a hole.

(iv) The density n_{se} of 2D electrons and the density n_{sh} of holes are reasonably high, giving rise to both intrasubband and intersubband transitions. The strong charge carrier–impurity scattering due to the presence of doping impurities in electron and hole layers gives rise to a large value of damping parameter for plasma oscillations. This is taken into account by choosing an appropriate form of 2D polarizabilities.

The remaining part of the paper is organized as follows. Section 2 deals with the calculation of the DDCF and the lineshapes. We present our results and their discussion in section 3. Finally, our work is summarized in section 4.

2. Density–density correlation function and the lineshapes

The lineshapes for different coupled plasmon–phonon modes can be determined from the imaginary part of the dynamical polarizability $\chi(q, \omega, z, z')$, which can be obtained by solving the integral equation [14]

$$\chi(q, \omega, z, z') = P(q, \omega, z, z') + \int\int dz_1\, dz_2\, P(q, \omega, z, z_1) V(q, z_1, z_2) \chi(q, \omega, z_2, z'). \quad (1)$$

Here, $P(q, \omega, z, z')$ is the polarizability in the absence of the Coulomb electron–electron interaction V. The phonon screened electron–electron interaction is given by [14]

$$V(q, z, z') = \frac{2\pi e^2}{q\varepsilon(\omega)} \exp(-q|z - z'|). \quad (2)$$

The $\varepsilon(\omega)$ for an infinite crystal can be given by

$$\varepsilon(\omega) = \varepsilon_\infty \frac{\omega^2 - \omega_{LO}^2 + i\gamma_{ph}\omega}{\omega^2 - \omega_{TO}^2 + i\gamma_{ph}\omega} \tag{3}$$

where ω_{LO} and ω_{TO} are the longitudinal optical and transverse optical phonon frequencies, respectively. ε_∞ is the optical dielectric constant and γ_{ph} is the phenomenological phonon linewidth.

We solve equation (1) for a GaAs DSSL by assigning the width d_e to an electron layer and the width d_h to a hole layer. The width of the undoped layer between an electron and a hole layer is taken to be d_i. The d is the sum of d_e, d_h and $2d_i$. The ordinate of the lth unit cell can be defined as

$$z = ld + R_j + t \qquad \text{with } -d_j/2 \leqslant t \leqslant d_j/2. \tag{4}$$

here R_j is the distance of the jth layer of the lth unit cell from the bottom of cell. j varies over the unit cell and can take two values. As has been mentioned earlier, both intrasubband as well as intersubband transitions are possible. One can use the diagonal approximation to decouple the different subband transitions [19]. Equation (1) can be transformed into [14, 15]

$$\chi_{ij}(q, \omega, l, l', t, t') = P_{ij}(q, \omega, t, t')\delta_{ll'}\delta_{ij}$$
$$+ \sum_{l_1, j'} \sum \int \int dt_1\, dt_2\, P_{ii}(q, \omega, t, t_1)V_{ij'}(q, l, l_1, t_1, t_2)\chi_{j'j}(q, \omega, l_1, t_2, t') \tag{5}$$

with

$$V_{ij}(q, l, l', t, t') = \frac{2\pi e^2}{q\varepsilon(\omega)} \exp[-q|(l - l')d + R_{ij} + (t - t')|] \tag{6}$$

where $R_{ij} = R_i - R_j$. χ_{ij} is a 2×2 matrix in i and j. Each element of matrix χ_{ij} is also a matrix. The size of the matrix is determined by the number of subbands which are to be considered in the calculation. For simplicity, we consider only two subbands (ground and first excited subband) and confined to the intrasubband transitions $(0 \to 0)$ within the ground subband and the intersubband transitions $(0 \to 1)$ between the ground subband and the first excited subband. Thus, each element of the matrix χ_{ij} decomposes into two terms, one of which corresponds to intrasubband transitions, while the other corresponds to the intersubband transitions. Equation (5) can now be simplified with the use of discrete Fourier transforms for obtaining the lineshapes of different coupled plasmon–phonon modes. The lineshapes can be given by [8, 15]

$$L(q, k_z, \omega) = \text{Im}[\chi_{ee}(q, \omega, k_z) + \chi_{eh}(q, \omega, k_z) + \chi_{he}(q, \omega, k_z) + \chi_{hh}(q, \omega, k_z)]. \tag{7}$$

Here k_z is the component of the wavevector along the direction of growth of the DSSL, while q is the component of the wavevector along the plane of an electron (hole) layer. Also, k_z is related to discrete variable l. In equation (7), χ_{ee} and χ_{hh} are the intralayer polarizabilities for electrons and for holes, respectively, while χ_{eh} and χ_{he} represent interlayer polarizabilities. Each of χ_{ee}, χ_{hh}, χ_{eh} and χ_{he} has two terms given by

$$\chi_{ij} = \sum_{\lambda=0}^{1} \chi_{ij}^{\lambda} \tag{8}$$

where λ is a composite subband index. The $\lambda = 0$ represents $0 \to 0$ transitions while $\lambda = 1$ represents $0 \to 1$ transitions. We obtain

$$\chi_{ee}^{\lambda} = -\frac{P_{ee}^{\lambda}(T_{hh}^{\lambda} - V_q P_{hh}^{\lambda} F_{hh}^{\lambda} W_{hh})A_{ee}^{\lambda}}{|\varepsilon^{\lambda}|} \tag{9a}$$

$$\chi_{eh}^\lambda = -\frac{V_q P_{ee}^\lambda F_{eh}^\lambda W_{eh} P_{hh}^\lambda A_{eh}^\lambda}{|\varepsilon^\lambda|} \tag{9b}$$

$$\chi_{he}^\lambda = -\frac{V_q P_{hh}^\lambda F_{hh}^\lambda W_{he} P_{ee}^\lambda A_{he}^\lambda}{|\varepsilon^\lambda|} \tag{9c}$$

$$\chi_{hh}^\lambda = \frac{P_{hh}^\lambda (T_{ee}^\lambda - V_q P_{ee}^\lambda F_{ee}^\lambda W_{ee}) A_{hh}^\lambda}{|\varepsilon^\lambda|} \tag{9d}$$

where

$$|\varepsilon^\lambda| = (T_{ee}^\lambda - V_q P_{ee}^\lambda F_{ee}^\lambda W_{ee})(T_{hh}^\lambda - V_q P_{hh}^\lambda F_{hh}^\lambda W_{hh}) - (P_{ee}^\lambda P_{hh}^\lambda V_q F_{eh}^\lambda V_q F_{he}^\lambda W_{eh} W_{he}) \tag{10}$$

with

$$V_q = 2\pi e^2/q\varepsilon(\omega) \tag{11}$$

$$T_{ii}^\lambda = 1 - V_q P_{ii}^\lambda (H_{ii}^\lambda - F_{ii}^\lambda). \tag{12}$$

In writing equations (8)–(12), we suppressed the explicit dependence on q, ω and k_z for brevity. W_{ee}, W_{hh}, W_{eh} and W_{he} are given by

$$W_{ij}(q, k_z) = \frac{\exp(-q|R_{ij}|)\exp(ik_z d)}{\exp(-ik_z d) - \exp(-qd)} + \frac{\exp(q|R_{ij}|)\exp(-qd)}{\exp(-ik_z d) - \exp(-qd)} \tag{13}$$

with $W_{ij}(q, k_z) \equiv W_{ji}(q, -k_z) \equiv W_{ji}^*(q, k_z)$ and $|R_{ee}| \equiv |R_{hh}| = 0$. The matrix elements $H_{ii}^\lambda(q)$, $F_{ij}^\lambda(q)$ and $A_{ij}^\lambda(k_z)$ are defined and are explicitly evaluated with the use of harmonic oscillator wavefunctions for both electrons and holes in the appendix.

P_{ee}^λ and P_{hh}^λ are non-interacting polarizabilities for 2D electron and hole gases, respectively. The existence of doping impurities in electron (hole) layers causes strong scattering centres for electrons (holes). In the presence of a random impurity potential, P_{ee}^λ and P_{hh}^λ for intrasubband transitions can be given by [18]

$$P_{jj}^0 = -N_{0j}\left[1 - \frac{\omega}{[(\omega + i\gamma_j)^2 - q^2 v_{Fj}^2]^{1/2} - i\gamma_j}\right] \tag{14}$$

where N_{0j} and γ_j are the density of states at the Fermi level and the damping constant, respectively. v_{Fj} is the Fermi velocity for electrons (holes). It should be mentioned that equation (14) is valid for $q < k_F$ and it reduces to the usual RPA 2D polarizability [19] for large ω- and small q-values. The intersubband transitions can be introduced through [11, 16]

$$P_{jj}^1 = \frac{2n_{sj}E_{10}}{E_{10j}^2 - \omega(\omega + (i\gamma_j))} \tag{15}$$

where E_{10j} is the energy band gap between the ground subband and the first excited subband of electrons or holes and it is defined as $E_{10j} = E_{1j} - E_{0j}$ with

$$E_{1j} = \frac{\hbar(4\pi e^2 N_{D/A})^{1/2}}{\varepsilon_\infty m_j^*}(1 + \tfrac{1}{2}) \tag{16}$$

$$E_{0j} = \frac{\hbar(4\pi e^2 N_{D/A})^{1/2}}{2\varepsilon_\infty m_j^*}. \tag{17}$$

E_{1j} and E_{0j} are the energy eigenvalues of the harmonic oscillator. $N_{D/A}$ is the number of donors or acceptors per unit volume.

3. Results and discussion

Equation (7) yields lineshapes of different plasmon–phonon-coupled modes. The maxima in $L(q, \omega, k_z)$ and zeros of $|\varepsilon^\lambda(q, \omega, k_z)|$ correspond to the frequencies of coupled plasmon–phonon modes. $|\varepsilon^\lambda(q, \omega, k_z)| = 0$ give rise to four roots of ω as a function of q and k_z, for each value of λ. For $\lambda = 0$, these are known as frequencies of coupled intrasubband hole plasmon–phonon modes (L_h^- and L_h^+) and of coupled intrasubband electron plasmon–phonon modes (L_e^- and L_e^+). The coupled modes of intersubband hole plasmons and phonons (I_h^- and I_h^+) and of intersubband electron plasmons and phonons (I_e^- and I_e^+) are obtained for $\lambda = 1$. The coupled plasmon–phonon modes are plotted as a function of qd for all possible values of $\cos(k_z d)$ in figure 1. For computation of these coupled modes, we used $\varepsilon_\infty = 10.9$, $d_e = 600$ Å, $d_h = 500$ Å, $d_i = 100$ Å, $m_e^* = 0.07m_e$, $m_h^* = 0.7m_e$, $N_A = N_D = 10^{18}$ cm^{-3}, $n_{se} = n_{sh} = 10^{12}$ cm^{-2}, $\gamma_{ph} = 0.1$ meV, $E_{10e} = 38.8$ meV, $E_{10h} = 12.3$ meV, $\omega_{LO} = 36.57$ meV and $\omega_{TO} = 33.845$ meV. γ_e and γ_h are estimated using $\gamma_j = e/m_j^* \mu_j$, where μ_j is the mobility. We estimate that $\gamma_e = 5$ meV and $\gamma_h = 4.5$ meV for the above-mentioned values of n_{se} and n_{sh} [3]. Each of L_h^-, L_e^-, I_h^-, L_h^+, L_e^+ and I_e^+ gives rise to a full band of frequencies, while I_e^- and I_h^+ do not form a band. L_e^- forms the widest band. All the plasmon modes in the L_h^- band and some plasmon modes in the L_e^- band are approximately proportional to $(q^2 - q_c^2)^{1/2}$ and they vanish as $q + q_c$, a critical value of q. The lower edge of the L_h^- and I_h^- bands corresponds to $k_z d = 0$, while that of the L_e^- and I_e^+ bands occur at $k_z d = \pi$. From the figure we notice that, for $k_z d \to 0$, the intrasubband plasmon modes of electron gas behave like the plasmons of a 3D free-electron gas and they are well defined even at $q \to 0$. On the other hand, none of intrasubband plasmons of hole gas behaves like the plasmon mode of a 3D free hole gas. It should be noted here that, for $k_z d \to 0$, the electron (hole) layers strongly interact with each other and a DSSL behaves like a two-component 3D free-carrier gas which yields one optical plasmon mode and one soft plasmon mode which goes to zero as $q \to q_c$. The L_h^- band is well separated from the L_e^- band. The L_h^+, L_e^+, I_h^+ and I_e^- bands originate from the interaction of GaAs phonons with different kinds of plasmon. The intrasubband and intersubband plasmons of the hole gas and the intrasubband plasmons of the electron gas interact weakly with phonons, while the intersubband electron plasmons interact strongly with phonons. Therefore, the bands of L_h^+, L_e^+ and I_h^+ almost overlap each other.

We have plotted $q_c d$ as a function of $k_z d$ for both electron and hole intrasubband plasmons in figure 2, with the use of the above-mentioned values for the parameters. It is seen from equations (10) and (13) that all possible values of $\cos(k_z d)$ lie in the $0 < k_z d < \pi$ range. The figure shows that $q_c d$ increases for electron intrasubband plasmons and decreases for hole intrasubband plasmons on increasing $k_z d$. For a hole gas, the $q_c d$-values are 1.66 and 1.45 at $k_z d = 0$ and $k_z d = \pi$, respectively, while, for an electron gas, $q_c d$ varies from zero to 0.45 for $0 < k_z d < \pi$. In a typical light-scattering experiment, $k_z \approx 7 \times 10^5$ cm^{-1}, which corresponds to $k_z d \approx 9.1$. Our calculation suggests that one cannot observe hole intrasubband plasmons for $q < 1.114 \times 10^5$ cm^{-1} and electron intrasubband plasmons for $q < 0.37 \times 10^5$ cm^{-1}, in a typical light-scattering experiment. It should be noted here that the value of the damping parameter also severely affects the q_c-value for the intrasubband plasmon mode. γ_h and γ_e are mainly governed by the doping impurity potential.

In figure 3, we have plotted the intrasubband plasma frequency as a function of damping parameter for both the electron and the hole gas for $qd = 1.47$ and $k_z d = 9.1$. The figure shows that the intrasubband plasmon energy decreases with increasing damping parameter and it vanishes at some critical value. The critical value of the hole intrasubband plasmon
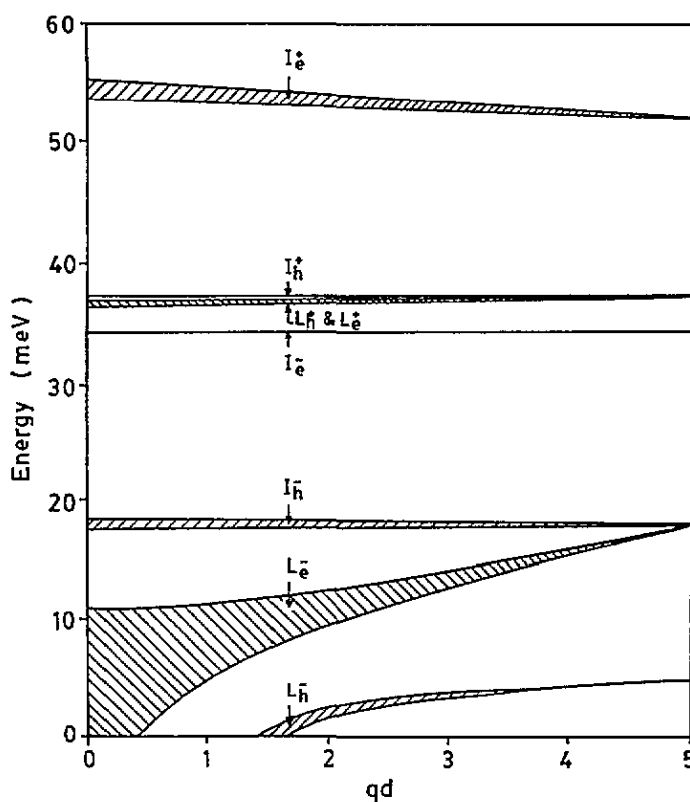
Figure 1. The coupled intrasubband plasmon–phonon modes (L_h^-, L_h^+, L_e^- and L_e^+) and the coupled intersubband plasmon–phonon modes (I_h^-, I_h^+, I_e^- and I_e^+).

mode is much smaller than that for the electron intrasubband plasmon mode. It should be mentioned that the carrier density and the damping parameter are related to each other. However, we have used a fixed value of $n_{se} \equiv n_{sh} = 10^{12}$ cm^{-2} to compute the curves which are shown in figure 3. The figure suggests that, for a given doping concentration, γ_h and γ_e should be tailored (via modulation of the space-charge potential and band edge of host material) in such a manner that one could observe well behaved intrasubband plasmons for both electrons and holes, in a typical light-scattering experiment. From the above discussions, we note that the strong charge carrier–impurity scattering (which is taken into account through polarizability and the matrix elements) severely affects the intrasubband plasmons.

The second term on the right-hand side of equation (10) describes the coupling between the plasma oscillations of the electron and hole gas. For $k_z d \to \pi$, the electron and hole gas layers couple loosely with each other and the plasma oscillations of each layer are almost independent of that of the others. The coupling betwen plasma oscillations of two adjoining electron and hole gas layers is negligibly small, for $k_z d = \pi$. On the other hand, the system exhibits a strong interaction between plasma oscillations of electron and hole gas layers (therefore the coupling term of equation (10) makes a substantial contribution) for $k_z d \to 0$. We have noticed that an analytical solution of equation (10) is not possible for $\lambda = 0$. In order to obtain further insight into the intrasubband plasmons, we consider a static limit of equation (3) and take a $k_z d \to \pi$ limit of equation (10). The intrasubband
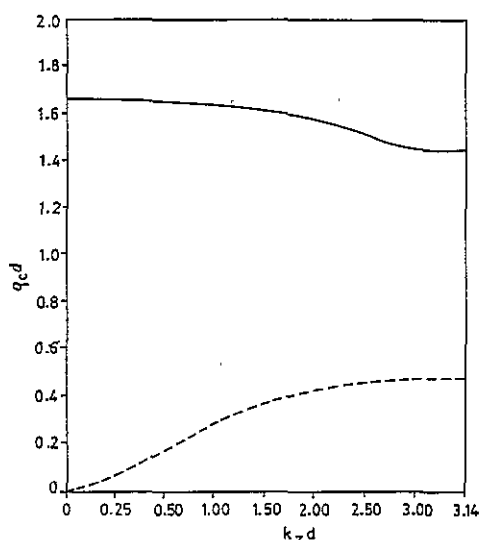
Figure 2. Critical q-values as a function of $k_z d$ for intrasubband plasmons of a hole gas (——) and an electron gas (- - - -).
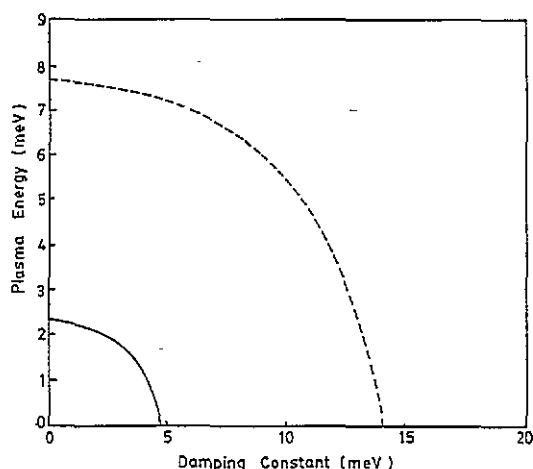
Figure 3. The intrasubband plasma energy as a function of the damping parameter for a hole gas (——) and an electron gas (- - - -), at $q = 1.13 \times 10^5$ cm^{-1} and $k_z = 7 \times 10^5$ cm^{-1}.

plasma frequency for the electron (hole) gas can now be given by

$$1 + \alpha_{jj}(q) P_{jj}^0(\omega) = 0 \tag{18a}$$

where

$$\alpha_{jj}(q) = \frac{2}{q \alpha_j^* \varepsilon_0} [H_{jj}^0(q) - F_{jj}^0(q)\{1 - S(q)\}]. \tag{18b}$$

Here, $\alpha_j^* = \hbar^2/m_j^* e^2$ is the effective Bohr radius for an electron (hole), ε_0 is the static value of equation (3) and $s(q)$ is defined by

$$S(q) = \frac{\sinh(qd)}{\cosh(qd) + 1}. \tag{18c}$$

Equation (18a) yields

$$\omega_{\rho j}(q) = \frac{1 + \alpha_{jj}}{1 + 2\alpha_{jj}} [\{q^2 v_{Fj}^2 (1 + 2\alpha_{jj}) - \gamma_j^2\}^{1/2} - i\gamma_j]. \tag{19}$$

Looking at equation (19), we note the following:

(i) $\omega_{\rho j}(q)$ acquires a wavevector-dependent imaginary part for a DSSL, which is not the case for a CSSL.

(ii) $\omega_{Pj}(q)$ is softened at small q, as its frequencies are lower than the corresponding frequencies for a CSSL, which can be given by $q^2 v_{Fj}^2 (1 + \alpha_{jj})^{1/2}$ in our notation.

(iii) $\omega_{\rho j}(q)$ exists for $q > q_c$ where q_c satisfies

$$q_c^2 v_{Fj}^2 (1 + 2\alpha_{jj}(q_c)) = \gamma_j^2. \tag{20a}$$

(iv) $\omega_{\rho j}(q)$ can be a well behaved plasmon mode if

$$q^2 v_{Fj}^2 [1 + 2\alpha_{jj}(q)] > 2\gamma_j^2. \tag{20b}$$

It should be mentioned here that one also obtains q_c defined by a equation similar to equation (20), even if one employs the usual RPA polarizability in place of that given by equation (14). It should be noted that some of the values of $q > q_c$ may not satisfy inequality (20b). Over such a q-range, plasma oscillations are not well defined and they lose their physical meaning. For a modulation doped CSSL, γ_j is very small (about 0.1 meV), giving rise to $q_c \approx 0$. One therefore can obtain well behaved acoustic plasmons in a CSSL at all small q-values. In order to look into the asymptotics of our results, we computed $\alpha_{jj}(q)$ as a function of q and have observed that $\alpha_{jj}(q)$ is almost independent of q for values of q close to q_c. It can be seen from equations (A7), (A9) and (18c) that, for small q-values, $F_{jj}^0 \sim H_{jj}^0 \sim 1$ and $S(q) \sim qd/2$, which gives rise to $\alpha_{jj}(q) \sim d/\alpha_j^* \varepsilon_0$. The asymptotic value of $\omega_{Pj}(q)$ can now be given by

$$\omega_{Pj}^\alpha(q) \sim \left[\frac{\pi n_{sj} e^2 d}{m_j^* \varepsilon_0} (q^2 - q_c^2) \right]^{1/2} \qquad (21a)$$

where

$$q_c \simeq \frac{\gamma_j}{(4\pi n_{sj} e^2 d/m_j^* \varepsilon_0)^{1/2}}. \qquad (21b)$$

For very small values of γ_j, $q_c \to 0$ and equation (21a) reduces to the well known result obtained for a CSSL [5, 11, 14]. Equation (21b) yields $q_c d = 0.45$ for electron plasmons and $q_c d = 1.37$ for hole plasmons.

The use of equation (15) to describe intersubband plasmons is well justified because it very well represents the intersubband transitions even for high values of γ_j. The effect of charge carrier–impurity scattering on intersubband plasmons has been incorporated in various matrix elements. The matrix elements, which are given in the appendix, significantly differ from the corresponding matrix elements which had been used for a modulation doped CSSL. The intersubband plasmons in a DSSL are well behaved for all $k_z d$-values.

We computed $L(q, \omega, k_z)$ as a function of ω for $q = 1.13 \times 10^5$ cm^{-1} and $q = 2 \times 10^5$ cm^{-1} for $k_z = 7 \times 10^5$ cm^{-1}. The values of other parameters are taken to be those used previously. Our computed $-\text{Im}[L(q, \omega, k_z)]$ are plotted in figure 4. The figure demonstrates that the line-shapes of L_h^-, L_e^-, I_h^-, I_e^- and L_e^+ are well resolved, while those of I_h^+, L_h^+ and L_e^+ overlap each other, for both q-values. The lineshapes at L_h^- and L_e^- (which correspond to intrasubband plamons) have a finite half-width and a reasonable peak height. All these lineshapes therefore could be observed in the light-scattering experiments.

Our calculation incorporates the background lattice vibrations in a phenomenological manner via equation (3). When the $\omega \to 0$ limit of equations (14) and (15) was substituted into equation (10), we obtain two values of ω on solving each of $|\varepsilon^0| = 0$ and $|\varepsilon^1| = 0$ for a given value of qd and of $k_z d$. These four values of ω correspond to the optical phonon frequencies of the polar GaAs lattice. Our computed optical phonon frequencies at $q = 2 \times 10^5$ cm^{-1} and $k_z = 7 \times 10^5$ cm^{-1} are 33.87 meV, 34.08 meV, 35 meV and 35.44 meV. The calculated phonon frequencies qualitatively agree with the bulk GaAs phonon frequencies observed in a recent light-scattering experiment performed on an ultrathin GaAs/AlAs superlattice [7]. It should be noted that most light-scattering experiments have been performed on GaAs/AlAs superlattices. The doped superlattices consist of homointerfaces while compositional superlattices such as GaAs/AlAs consist of heterointerfaces. A GaAs/AlAs superlattice supports both bulk as well as interface phonons, while the doped GaAs superlattice can support bulk phonon modes.
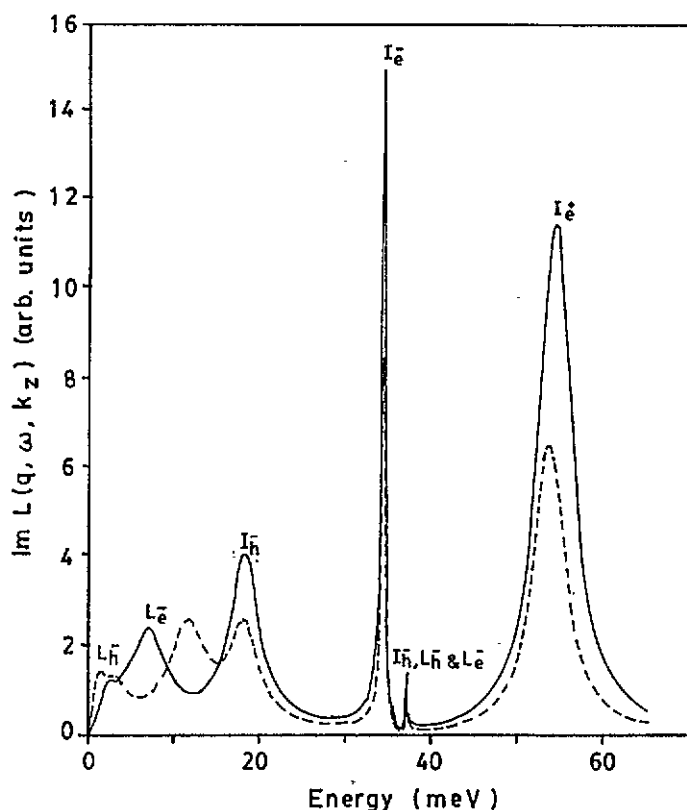
Figure 4. Plot of $-\mathrm{Im}(q, \omega, k_z)$ as a function of ω for $q = 1.13 \times 10^5$ cm^{-1} (————) and for $q = 2 \times 10^5$ cm^{-1} (- - - -) at $k_z = 7 \times 10^5$ cm^{-1}.

4. Conclusions

We performed a model calculation of DDCF for a GaAs DSSL to study the plasmon–phonon-coupled modes and the lineshapes of coupled modes by taking into account the strong charge carrier–impurity scattering from the potential of the random impurities and the diffusive nature of the boundaries of the electron (hole) layers. Our model calculation demonstrates that the strong scattering of electrons (holes) from doped impurities has a marked influence on both the intrasubband and the intersubband plasmons in a DSSL. The plasmons of a DSSL significantly differ from electron (hole) plasmons in a modulation doped CSSL such as $Ga_x In_{1-x} As/GaAs_y Sb_{1-y}$. The intrasubband plasmon frequency for a DSSL has a wavevector-dependent imaginary part which can become comparable with the real part, for certain values of q and k_z. For this case, plasma oscillations are not well defined and they lose their physical meaning. It is very unlikely that any of the plasmon modes of a DSSL behave like an acoustic plasmon mode because of the high value of the damping parameter. q_c is always smaller for electron plasmons than for hole plasmons. The positions and peak heights of the lineshapes of hole plasmons are smaller than those of electron plasmons. For the right choice for the values of the DSSL parameters, the lineshapes of different coupled plasmon–phonon modes are well separated from each other.

These lineshapes could be observed in a typical light-scattering experiment on a GaAs DSSL.

Acknowledgments

Appendix

$A_{ij}^{\lambda}(k_z)$ is defined as

$$A_{ij}^{\lambda}(k_z) = \int_{-d_i/2}^{d_i/2} \exp(-\mathrm{i}k_z t)\psi_i^{\lambda}(t)\,\mathrm{d}t \int_{-d_j/2}^{d_j/2} \exp(-\mathrm{i}k_z t')\psi_i^{\lambda}(t')\,\mathrm{d}t' \tag{A1}$$

while the matrix elements $H_{ij}(q)$ are given by

$$H_{ij}^{\lambda}(q) = \int_{-d_i/2}^{d_i/2} \mathrm{d}t \int_{-d_j/2}^{d_j/2} \mathrm{d}t'\,\exp(-q|t - t'|)\psi_i^{\lambda}(t)\psi_j^{\lambda}(t'). \tag{A2}$$

Here $\psi_i^{\lambda}(t)$ is the product of two envelope functions. F_{ij} is given by equation (A2) on replacing $q|t - t'|$ by $q(t - t')$. A_{ee}^{λ}, A_{hh}^{λ}, A_{eh}^{λ}, A_{he}^{λ}, H_{ee}^{λ}, H_{hh}^{λ}, F_{ee}^{λ}, F_{eh}^{λ}, F_{he}^{λ} and F_{hh}^{λ} are evaluated using the envelope functions.

$$\psi_j^0 = |\phi_j^0|^2 \qquad \psi_j^1 = \phi_j^1\phi_j^0 \tag{A3}$$

where ϕ_j^n are the harmonic oscillator wave functions, which can be given by

$$\phi_j^n = N^n \exp(-\alpha_j z^2/2)H^n(\alpha_j) \tag{A4}$$

with

$$N^n = \left(\frac{\alpha_j}{2^n\sqrt{\pi}\,n!}\right)^{1/2}. \tag{A5}$$

α_j is defined by

$$\alpha_j = \left(\frac{4\pi e^2 m_j^* N_{D/A}}{\hbar^2\varepsilon_{\infty}}\right)^{1/4}. \tag{A6}$$

On performing the integration in equations (A1) and (A2) with the use of equations (A3) and (A4) we obtain

$$F_{ij}^0(q) = \exp\left[\frac{q^2}{4}\left(\frac{1}{\alpha_i^2} + \frac{1}{\alpha_j^2}\right)\right] \tag{A7}$$

$$F_{ij}^1(q) = -\frac{q^2}{2\alpha_i\alpha_j}\exp\left[\frac{q^2}{4\alpha_i^2} + \frac{q^2}{4\alpha_j^2}\right] \tag{A8}$$

$$H_{jj}^0(q) \simeq \exp(q^2/\alpha_j^2) - (\sqrt{2}q/\sqrt{\pi}\alpha_j)\exp[-q^2/2\alpha_j^2] \tag{A9}$$

$$H_{jj}^1(q) \simeq (q/2\sqrt{\pi})(2.122q^2/\alpha_j^3 + \sqrt{2}/\alpha_j)\exp[-q^2/2\alpha_j^2] - (q^2/2\alpha_j^2)\exp[q^2/2\alpha_j^2]. \tag{A10}$$

A_{ij}^0 and A_{ij}^1 can be obtained from equations (A7) and (A8), respectively, on replacing q by $\mathrm{i}k_z$.

References

[1] Döhler G H 1972 *Phys. Status Solidi* b **52** 79–92 .
[2] Döhler G H 1972 *Phys. Status Solidi* b **52** 533–45
[3] Ploog K and Döhler H 1983 *Adv. Phys.* **32** 285–359
[4] Döhler G H 1992 *Proc. Conf. on the Physics and Technology of Semiconductor Device and Integrated Circuits (Proc. SPIE 1523)* (Bellingham, WA: SPIE) pp 23–63
[5] Olegao D, Pinczuk A, Gossard A C and Wiegman W 1982 *Phys. Rev.* B **26** 7867–9
[6] Sorayakumar R, Pinczuk A, Gossard A C and Wegmann W 1985 *Phys. Rev.* B **31** 2578–80
[7] Scamarcio G, Haines M, Abstreiter G, Molinari E, Baroni S, Fischer A and Ploog K 1993 *Phys. Rev.* B **47** 1483–99
[8] Tozoar N and Zhang C 1986 *Phys. Rev.* B **34** 1050–6
[9] Sharma A C 1991 *Mod. Phys. Lett.* B **5** 455–63
[10] Jain J K and Allen P B 1985 *Phys. Rev. Lett.* **54** 947–1004
[11] Tselis A C and Quinn J J 1984 *Phys. Rev.* B **29** 3318–25
[12] Bloss W L and Brody E M 1982 *Solid State Commun.* **43** 523–8
[13] Camley R E and Mills D L 1984 *Phys. Rev.* B **29** 1695–706
[14] Katayama S and Ando T 1985 *J. Phys. Soc. Japan* **54** 1615–26
[15] Sharma A C and Sood A K 1994 *J. Phys.: Condens. Matter* **6** 1553–62
[16] Hawrylak P, Wu J and Quinn J J 1985 *Phys. Rev.* B **32** 5169–76
[17] Ruden P and Dohler G H 1983 *Phys. Rev.* B **27** 3538
[18] Giuliani G F and Quinn J J 1983 *Phys. Rev.* B **29** 2321–3
[19] Dahl D L and Sham L J 1977 *Phys. Rev.* B **16** 651–69